Report

SOURCE DATA | TRANSPARENT PROCESS

EMBO reports

Requirements for multivalent Yb body assembly in transposon silencing in *Drosophila*

Shigeki Hirakata, Hirotsugu Ishizu†, Aoi Fujita, Yumiko Tomoe & Mikiko C Siomi*

Abstract

Female sterile (1) Yb (Yb) is a primary component of Yb bodies, perinuclear foci considered to be the site of PIWI-interacting RNA (piRNA) biogenesis in *Drosophila* ovarian somatic cells (OSCs). Yb consists of three domains: Helicase C-terminal (Hel-C), RNA helicase, and extended Tudor (eTud) domains. We previously showed that the RNA helicase domain is necessary for Yb–RNA interaction, Yb body formation, and piRNA biogenesis. Here, we investigate the functions of Hel-C and eTud and reveal that Hel-C is dedicated to Yb–Yb homotypic interaction, while eTud is necessary for Yb–RNA association, as is the RNA helicase domain. All of these domains are indispensable for Yb body formation and transposon-repressing piRNA production. Strikingly, however, genic piRNAs unrelated to transposon silencing are produced in OSCs where Yb bodies are disassembled. We also reveal that Yb bodies are liquid-like multivalent condensates whose assembly depends on Yb–Yb homotypic interaction and Yb binding particularly with *flamenco* RNA transcripts, the source of transposon-repressing piRNAs. New insights into Yb body assembly and biological relevance of Yb bodies in transposon silencing have emerged.

Keywords female sterile (1) Yb; liquid–liquid phase separation; piRNA; transposon; Yb body

Subject Categories Chromatin, Epigenetics, Genomics & Functional Genomics; RNA Biology; Transcription

DOI 10.15252/embr.201947708 | Received 10 January 2019 | Revised 14 April 2019 | Accepted 16 April 2019 | Published online 30 April 2019

EMBO Reports (2019) 20: e47708

Introduction

PIWI-interacting RNAs (piRNAs) are engaged in an arms race with mobile transposons to maintain the genetic integrity of the germline [1–6]. In *Drosophila* ovarian somatic cells (OSCs), transposon-repressing piRNAs arise nearly exclusively from the uni-strand piRNA cluster *flamenco* (*flam*), located at the pericentromeric region of the X chromosome [7–10]. Upon transcription, the *flam* RNA transcripts undergo partial splicing and are exported to the cytoplasm, where they accumulate into the perinuclear structures Flam bodies/Dot COM for further processing [11–13]. The *flam*-piRNA precursors may also be stored at nuclear Dot COM prior to nuclear export [14].

piRNA processing in OSCs occurs in a manner dependent on a number of piRNA factors [15–22]. Upon processing, mature piRNAs form piRNA-induced silencing complexes (piRISCs) with Piwi, a member of the PIWI protein family in *Drosophila*. The other two PIWI members, Aubergine and Ago3, are not expressed in OSCs. Piwi-piRISCs are then imported to the nucleus by Importin α [23], where they repress transposons cotranscriptionally with multiple cofactors such as Gtsf1/Asterix, Maelstrom, Histone H1, HP1a, Eggless/dSetDB1, and Panoramix/Silencio [24–31].

Yb bodies are gonadal soma-specific membraneless organelles [16,32] to which piRNA biogenesis factors, female sterile (1) Yb (Yb), Armitage (Armi), Sister of Yb (SoYb), Vreteno (Vret), and Shutdown (Shu) are localized [15–17,19,32]. Loss of these factors abrogates piRNA biogenesis; thus, Yb bodies are considered to be the site of piRNA production. Other processing factors, Zucchini (Zuc), Gasz, and Minotaur (Mino), are not localized to Yb bodies but are anchored on the surface of mitochondria through their own transmembrane signals [16,21,22]. Yb bodies tend to be surrounded by mitochondria and adjacent to Flam bodies [12,32]. This spatial arrangement of the organelles locally concentrates piRNA-processing factors and precursor RNAs, facilitating piRNA biogenesis and Piwi-piRISC formation. The hierarchy of Yb body assembly has previously been examined [16,17,19]. However, a comprehensive and systematic analysis including SoYb has not been performed.

Yb contains three functional domains: Helicase C-terminal (Hel-C), RNA helicase, and extended Tud (eTud) domains [17,32]. The RNA helicase domain consists of P-loop NTPase and Hel-C domains. We previously showed that alteration of Gln399 or Asp537 in the RNA helicase domain to alanine severely reduced the RNA-binding activity of Yb [12]. Both mutants Q399A and D537A failed to form Yb bodies and barely restored the piRNA biogenesis and transposon silencing abrogated by loss of endogenous Yb in OSCs. This suggested that the association of Yb with piRNA precursors via the RNA helicase domain is essential for Yb body formation and piRNA biogenesis.

The *cis*-elements that drive piRNA biogenesis were identified in *flam* transcripts and genic piRNA sources such as *traffic jam* (*tj*) mRNAs [33,34]. Enforced tagging of the *cis*-element to the 5′ end,

Department of Biological Sciences, Graduate School of Science, The University of Tokyo, Tokyo, Japan
*Corresponding author. Tel: +81 3 5841 4386; E-mail: siomim@bs.s.u-tokyo.ac.jp
†Present address: Department of Molecular Biology, Keio University School of Medicine, Tokyo, Japan

but not the 3′ end, of arbitrary RNAs induced artificial piRNA production from the downstream regions, which repressed genes highly complementary to the piRNAs [33,34]. Yb acts as the *trans*-acting factor, binding to the *cis*-element and triggering piRNA biogenesis. RNA binding of Yb also determines the regions from which piRNAs are produced [34,35]. Yb is not involved in the transcription of *flam* and possibly genic piRNA sources [36].

Both the Hel-C and the eTud domains of Yb are necessary for *piwi* and *hedgehog* expression in ovarian cap cells and for germarium development [32]. However, their molecular functions in piRNA biogenesis remain elusive. In this study, we produced two Yb deletion mutants, ΔHel-C and ΔeTud, and analyzed them biochemically, which revealed that Hel-C is necessary for self-association of Yb while eTud is essential for Yb to interact with piRNA precursors and Armi. Armi is required for localizing the SoYb–Vret heterodimer to Yb bodies, and all three domains of Yb are necessary for Yb body assembly and transposon silencing. The production of *flam*-piRNAs was severely impaired by the loss of Hel-C and eTud, leading to transposon derepression. Strikingly, however, non-transposon-repressing genic piRNAs, whose functions remain rather unclear, were expressed in OSCs lacking Hel-C, but not those lacking eTud. Similar phenotypes were observed in *flam* mutants where the transcription of *flam* was impaired. We also found that Yb bodies had properties compatible with liquid-like phase separation. In summary, Yb bodies are multivalent RNA–protein condensates whose assembly depends both on homotypic interaction of Yb through the Hel-C domain, and on Yb binding *flam* RNAs. Yb body formation is not absolutely required for piRNA biogenesis. However, without Yb bodies, transposon-repressing piRNAs are scarcely produced, resulting in the failure of transposon repression. The biological relevance of Yb/*flam*-driven Yb body assembly in the somatic piRNA pathway has now emerged.

Results and Discussion

Determination of the hierarchical manner of Yb body assembly

To understand the hierarchy of protein components in Yb body assembly, we produced anti-SoYb and anti-Vret monoclonal antibodies (Fig EV1A) and conducted biochemical analyses. Ectopically expressed Shu in OSCs was cytosolic and failed to localize to Yb bodies (Fig EV1B). We inferred that Shu may not be a constitutive component of Yb bodies, so excluded the protein from the following analyses. Immunoprecipitation followed by Western blotting demonstrated that the Armi and Vret complexes immunoisolated from OSCs contained Yb/SoYb/Vret and Yb/Armi/SoYb, respectively (Fig 1A and B). Two isoforms of Armi were detected as a doublet in Western blotting, as previously reported [15]. Silver staining of protein components of the Vret complex is shown in Fig 1C.

We repeated the experiments in OSCs where individual components had been downregulated by RNAi. Armi, SoYb, and Vret associated with each other even in the absence of Yb (Fig 1D). Upon Armi depletion, SoYb and Vret continued to interact but failed to coimmunopurify with Yb, suggesting that SoYb and Vret heterodimerize in an Armi-independent manner and that the heterodimer associates with Yb in an Armi-dependent manner (Fig 1E). Depletion of SoYb and Vret had little impact on Yb–Armi association (Fig 1D). When Vret was depleted, the abundance of SoYb was reduced (Figs 1D and EV1C). Similarly, the level of Vret decreased upon SoYb loss. It seems that SoYb and Vret stabilize each other via a physical protein–protein interaction.

Immunofluorescence confirmed that all of these components localize to Yb bodies in OSCs (Figs 1F and EV1D). Yb bodies disappeared upon the loss of Yb, and the other components were dispersed in the cytosol (Fig 1F). Without Armi, Yb bodies appeared, but SoYb and Vret remained cytosolic. When SoYb and Vret were depleted, Armi localized to Yb bodies (Fig 1F). Residual SoYb in Vret-lacking OSCs failed to localize to Yb bodies and *vice versa*. The hierarchical manner of Yb body assembly is suggested: Yb triggers Yb body formation in a manner independent of Armi, SoYb, and Vret. Armi then joins the foci via a physical interaction with Yb. At this step, Armi may or may not be accompanied by SoYb and Vret. Finally, the SoYb–Vret heterodimer localizes to Yb bodies by interacting with Armi (Fig 1G). Depletion of Shu had little impact on Yb body localization of Armi, SoYb, and Vret (Fig EV1E). Yb may or may not require other factors to initiate the process of Yb body formation. Further analysis to address this is anticipated.

The Hel-C and eTud domains of Yb are required for Yb self-association and interaction with other Yb body components, respectively

To understand the functions of the Hel-C and eTud domains of Yb, we produced two deletion mutants, ΔHel-C and ΔeTud, and examined their biological properties. The ΔHel-C mutant lacks the N-terminal 150 amino acids (1–150) that include the Hel-C domain (33–133), while the ΔeTud mutant lacks the 218 most C-terminal amino acids (825–1,042) involving the eTud domain (825–1,014; Figs 2A and EV2A).

We conducted immunoprecipitation in OSCs in which endogenous Yb had been knocked down by RNAi. Western blotting showed that both wild-type (WT) Yb and the ΔHel-C mutant interacted with Armi, but ΔeTud did not (Fig 2B), suggesting that Yb associates with Armi through the eTud domain. In normal OSCs in which endogenous Yb was present, ΔeTud showed greatly reduced binding of Armi (Fig 2C). However, the mutant did associate with endogenous Yb. In contrast, the ΔHel-C mutant behaved in the completely opposite manner: ΔHel-C associated with Armi but not with endogenous Yb (Fig 2C). These results indicate that the Hel-C domain acts as a self-association domain of Yb, while eTud serves as the Armi-interacting domain. Because the SoYb–Vret heterodimer bound with Yb in an Armi-dependent manner (Fig 1E), eTud is also considered to be the domain for the recruitment of SoYb–Vret heterodimer to the Yb complex.

Flag- and Myc-tagged Hel-C domains that were simultaneously expressed in OSCs copurified (Figs 2D and EV2B). Thus, the Hel-C domain is both necessary and sufficient for Yb–Yb interaction.

Yb body formation requires both Hel-C and eTud in addition to the RNA helicase domain

We next examined the subcellular localization of the ΔHel-C and ΔeTud mutants in Yb-lacking OSCs (Fig 2E). Yb bodies appeared when WT Yb was expressed by transfection, to which endogenous

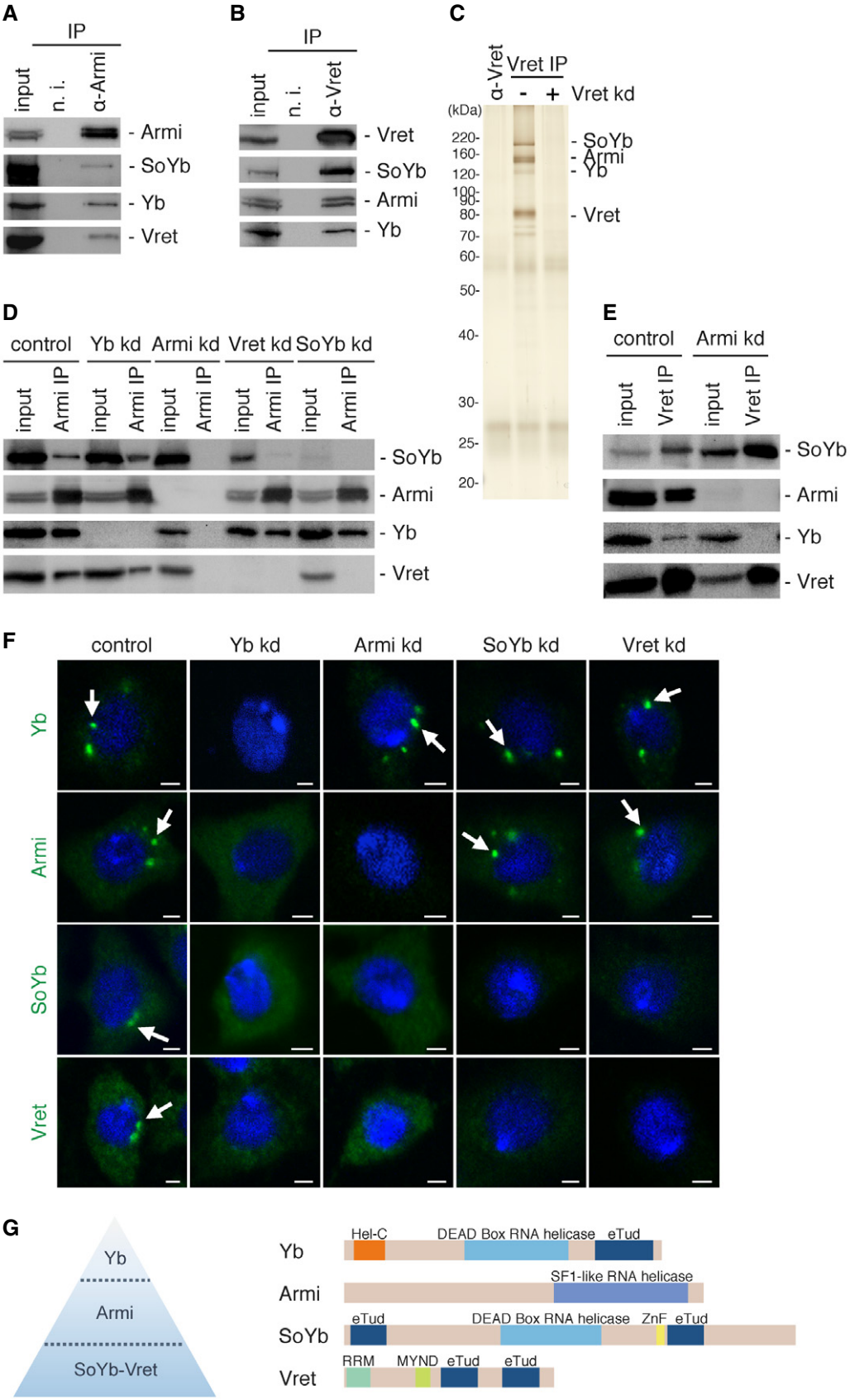

Figure 1.

Figure 1. Hierarchy of protein components in Yb body assembly.

A The Armi complex immunoisolated from OSCs using anti-Armi antibodies contains Yb, SoYb, and Vret.

B The Vret complex immunoisolated from OSCs using anti-Vret antibodies contains Yb, Armi, and SoYb.

C Silver staining of protein components in the Vret complex in (B). The lane α-Vret (left) contained only the anti-Vret antibodies used in these experiments.

D Immunoprecipitation and Western blotting were performed in OSCs upon RNAi treatment (kd). Even without the association of Yb, Armi, SoYb, and Vret associated. Yb and Armi remained bound to each other upon SoYb or Vret depletion. The level of SoYb (input) decreased upon Vret depletion. Likewise, the level of Vret (input) decreased upon SoYb depletion.

E Upon Armi depletion, SoYb and Vret were still bound to each other but this heterodimer no longer associated with Yb.

F Immunofluorescence analyses in OSCs. Yb bodies disappeared upon Yb depletion, which led Armi, SoYb, and Vret to be localized in the cytosol. Yb bodies were detected in OSCs upon Armi depletion, but SoYb and Vret localized in the cytosol. Armi was detected at Yb bodies upon SoYb or Vret depletion. Yb bodies are indicated by white arrows. Nuclei are shown in blue. Scale bar: 2 μm.

G The hierarchy of Yb body assembly proposed in this study. Domain structures of Yb, Armi, SoYb, and Vret are shown on the right. Hel-C, Helicase C-terminal; eTud, extended Tudor; ZnF, zinc finger; RRM, RNA-recognition motif; MYND, MYND-type zinc finger.

Source data are available online for this figure.

Armi colocalized. In contrast, both Yb mutants failed to assemble punctate structures and instead scattered evenly in the cytosol. In both cases, endogenous Armi remained dispersed in the cytosol. Therefore, both the Hel-C and the eTud domains are necessary for Yb body formation, as is the RNA helicase domain [12], although their functions are clearly distinct.

Yb formed Yb bodies in Armi-lacking OSCs (Fig 1F in this study and Ref. [16]), meaning that the Yb–Armi interaction is dispensable for Yb body formation. Therefore, eTud has other function(s) besides binding Armi. We conducted UV cross-linking and immunoprecipitation (CLIP) to examine the RNA-binding activity of ΔeTud and ΔHel-C. While the ΔHel-C mutant was capable of binding RNAs to an extent similar to that of WT Yb, the ΔeTud mutant had no such activity (Fig 2F). Thus, the eTud domain is required for Yb–RNA association and Yb body assembly in a coordinated manner with the RNA helicase domain. How the eTud domain exhibits the RNA binding remains unknown. The eTud domain is composed of an authentic Tud domain and a nuclease-like domain [17], the latter of which may contribute to the RNA binding. Alternatively, some unknown factor(s) responsible for the activity binds eTud.

Yb body formation is required for producing transposon-repressing piRNAs but unnecessary for producing non-transposon-repressing genic piRNAs

We inferred that the ΔeTud mutant would not rescue defects in piRNA biogenesis caused by loss of endogenous Yb because of its lack of RNA-binding activity. As expected, ΔeTud failed to recover the piRNA levels (Fig 3A). However, under the same conditions, the ΔHel-C mutant expressed piRNAs to an extent similar to that of the WT Yb control (Figs 3A and EV3A). Piwi was detected in the nucleus of OSCs when ΔHel-C was expressed instead of endogenous Yb (Fig EV3B), indicating that Piwi was mostly loaded with piRNAs. Strikingly, however, transposons remained expressed at high levels even after ΔHel-C expression (Fig 3B). The most likely explanation for this is that the piRNA population was drastically changed by the lack of the Hel-C domain.

To test this possibility, we sequenced and compared piRNAs produced in both the presence and the absence of Hel-C. This revealed that a lack of Hel-C greatly reduced the levels of *flam*-piRNAs while the abundance of *tj*-piRNAs was maintained (Fig 3C and D, and Table EV1). It should be noted that in both cases, the mapping patterns throughout the loci were only slightly impacted by the loss of Hel-C, suggesting that the Hel-C domain does not contribute to determining the specificity of Yb–RNA binding. More comprehensive analysis revealed that the percentage of transposon-repressing piRNAs in the total reads became much lower when Hel-C was missing (Figs 3E and EV3C). In contrast, the percentage of genic piRNAs apparently increased. However, the Spearman's rho of non-transposon-repressing piRNAs was maintained at 0.96 even upon the Hel-C deletion (Fig 3E). This also supports the idea that the Hel-C domain contributes only slightly to determining the specificity of Yb–RNA binding. The specificity of Yb–RNA binding is therefore governed by the RNA helicase and eTud domains.

CLIP-qPCR confirmed that Yb–*flam* RNA interaction was severely attenuated by the lack of the Hel-C domain (Fig 3F). In contrast, the activity of Yb to interact with genic piRNA precursors, including *dm*, *c-Fos*, and *CG9257* mRNA, was hardly impacted by the loss of Hel-C. This means that, under conditions where the Yb–*flam* RNA interaction was severely attenuated, Yb bound more abundantly with genic piRNA sources. This explains the increased level of genic piRNAs in Fig 3E. Such relative increase was not observed for *tj*-piRNAs (Fig 3D). This was likely due to the relatively high abundance of *tj*-piRNAs among genic piRNAs in normal OSCs. In that case, the discrepancy in the presence and absence of the Hel-C domain may not be very obvious.

Genic piRNAs show little or no complementarity to transposons or any other genes expressed in OSCs and so are "useless" for the regulation of gene expression. This explains why the expression levels of transposons remained high in the context of lack of Hel-C with a low abundance of *flam*-piRNAs. The functions of the three domains of Yb are summarized in Fig 3G. The most important key point here is that the Hel-C domain of Yb is essential for increasing the stability of Yb-*flam* RNA binding but not essential for Yb-mRNA (genic piRNA sources) binding. Therefore, in the absence of Hel-C, transposon-repressing piRNA production is specifically attenuated.

Yb bodies are phase-separated condensates whose assembly depends on Yb and *flam* transcripts

Cytoplasmic membraneless organelles such as P bodies and P granules are composed of RNAs and RNA-binding proteins and show propensities comparable to liquid–liquid phase separation (LLPS) [37]. P bodies sequester translationally repressed mRNAs to increase their stability [38]. P granules are germline-specific structures necessary for germline development in *C. elegans* [39]. Yb bodies are also cytoplasmic membraneless organelles found specifically in germline cells. Therefore, we postulated that Yb bodies

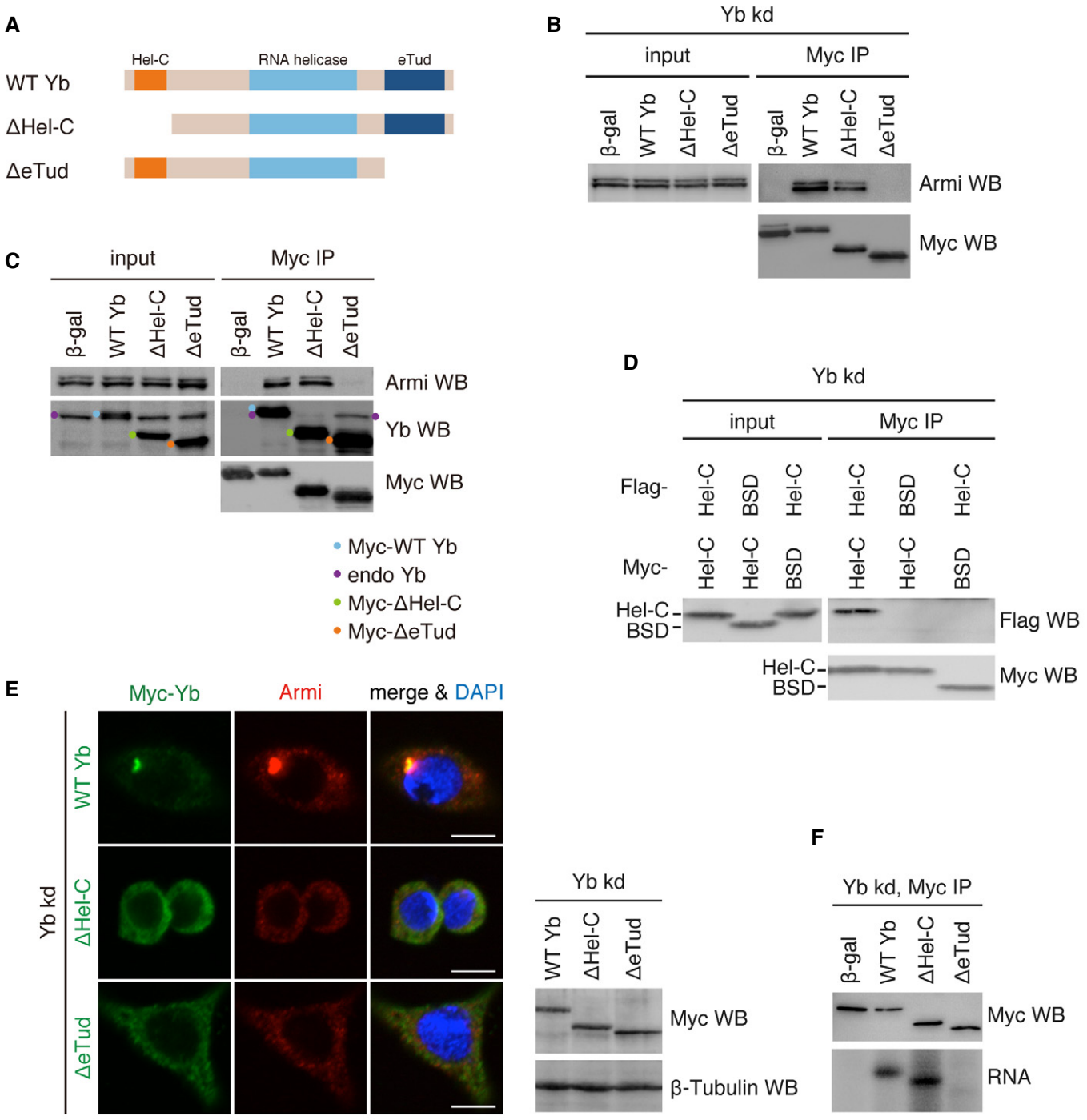

Figure 2. Behaviors of Yb mutants ΔHel-C and ΔeTud in OSCs.

A Domain structures of WT Yb and deletion mutants ΔHel-C and ΔeTud.

B In Yb-lacking OSCs (Yb kd), WT Yb and ΔHel-C bound to Armi but ΔeTud did not. Note that WT Yb and both mutants were engineered to be RNAi-resistant by mutations. β-gal was used as a negative control.

C In normal OSCs, WT Yb and ΔeTud bound with Yb but ΔHel-C did not.

D Flag-Hel-C copurified with Myc-Hel-C but not with blasticidin S deaminase (BSD; negative control).

E Subcellular localization of WT Yb and deletion mutants ΔHel-C and ΔeTud. Myc-Yb is shown in green. Endogenous Armi is shown in red. DAPI shows nuclei (blue). Scale bar: 5 μm. Western blotting (right) showing WT Yb and deletion mutants ΔHel-C and ΔeTud expressed in Yb-lacking OSCs.

F CLIP shows that WT Yb and ΔHel-C bind RNA *in vivo* but ΔeTud does not.

Source data are available online for this figure.

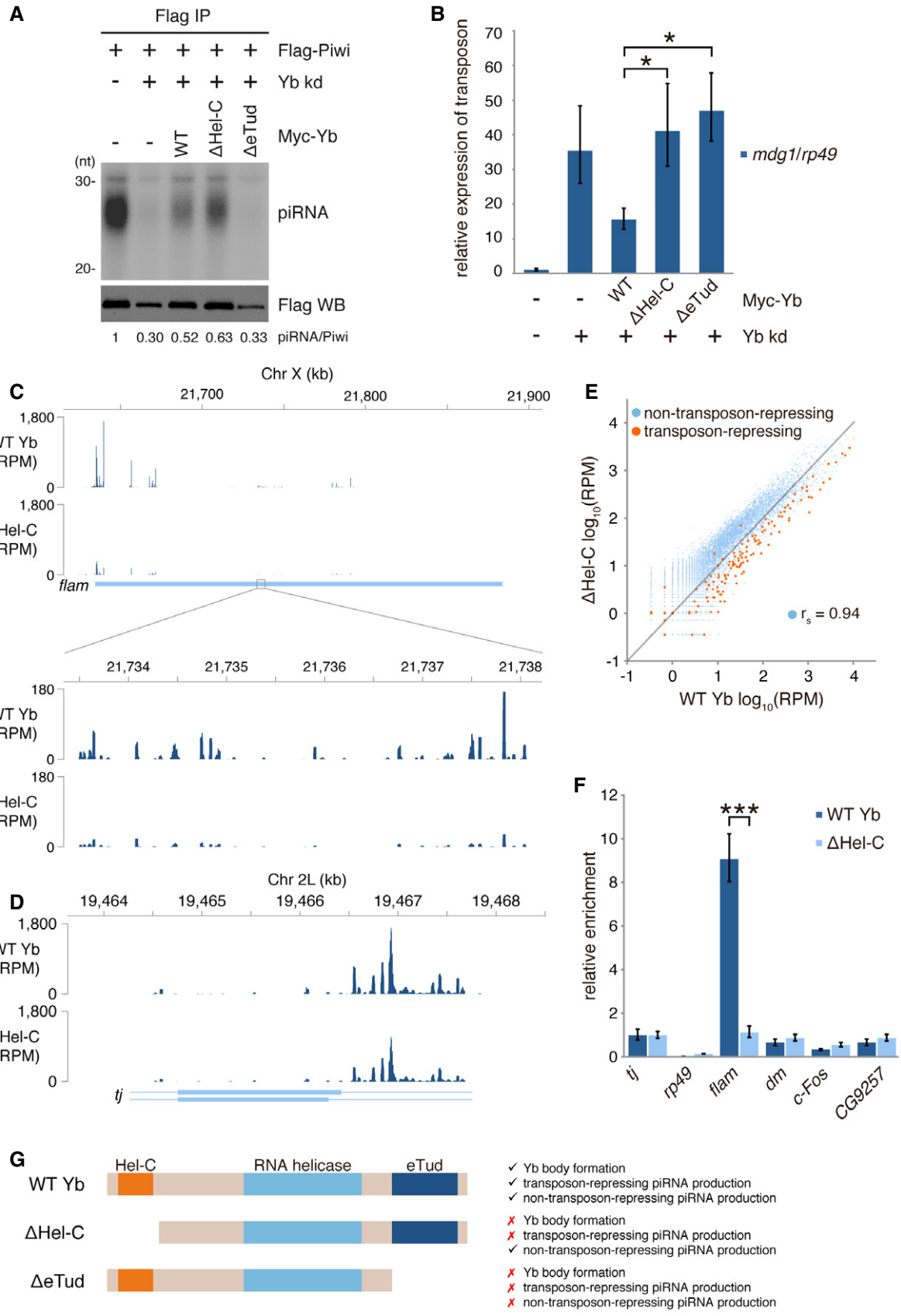

Figure 3.

Figure 3. Functional analyses of ΔHel-C and ΔeTud.

A Rescue experiments showing that ΔHel-C but not ΔeTud restored piRNA biogenesis attenuated by endogenous Yb depletion. Flag-Piwi was expressed upon endogenous Yb depletion.

B The levels of transposon *mdg1* in (A). Bars and error bars represent means ± SEM values of three independent experiments. *P*-values were calculated by *t*-test. $*P < 0.05$.

C Mapping of *flam*-piRNAs produced in the presence and absence of the Hel-C domain in OSCs.

D Mapping of *tj*-piRNAs produced in the presence and absence of the Hel-C domain in OSCs.

E Scatterplot showing changes in the abundances of transposon-repressing piRNAs and non-transposon-repressing piRNAs in the presence and absence of the Hel-C domain. Orange and blue dots indicate the number of normalized piRNA reads mapped uniquely to transposons in the reverse orientation and coding genes in the sense orientation, respectively.

F The relative enrichments of RNAs coimmunopurified with WT Yb and ΔHel-C. Bars and error bars represent means ± SEM values of three independent experiments. In addition to *tj*, three genic piRNA sources that were characterized in previous studies (*dm/Myc* [59], *c-Fos/kay* [60], and *CG9257* [34]) are also shown. *rp49* was used as a negative control. *P*-value was calculated by *t*-test. $***P < 0.001$.

G Summary of requirements of Hel-C and eTud domains of Yb in Yb body formation and transposon-repressing and non-transposon-repressing piRNA production.

Source data are available online for this figure.

might also be formed by phase separation. To test this, we treated OSCs with 1,6-hexanediol, a small compound that disrupts LLPS *in vivo*. Yb bodies disappeared upon treatment, as did P bodies (Fig 4A). Live imaging of GFP-fused Yb in OSCs showed that the condensates moved around dynamically in the cytosol (Movie EV1). Fusion- and fission-type phenomena, which are common in liquid-like condensates, were also observed (Fig 4B and Movie EV1). Based on these observations, we judged that Yb bodies are formed by LLPS.

Liquid–liquid phase separation takes place based on protein–protein interactions through prion-like domains or intrinsically disordered regions (IDRs) [37]. However, upon the application of PLAAC for searching for prion-like domains in proteins, it was predicted that Yb has no such domain. PONDR-FIT, a predictor of IDRs, indicated that Yb has an IDR between the Hel-C and RNA helicase domains (Figs EV2A and EV4A). Curiously, however, the Hel-C domain was not predicted to be an IDR (Fig EV4A). IDRs normally contain repetitive amino acid sequences rich in aromatic residues [37]. The Hel-C domain is not repetitive, but is rich in aromatic residues (~10%). Four of the residues, Tyr23, Trp91, Tyr95, and Phe129, are highly conserved in the members of the *Drosophila melanogaster* group (Fig EV4B). We individually mutated Tyr23 and Phe129 to alanine and found that these alterations impaired Yb body assembly (Fig 4C). Both mutants Y23A and F129A failed to produce *flam*-piRNAs in Yb-depleted OSCs, as did the ΔHel-C mutant (Fig 4D). The mutations greatly reduced interaction with WT Yb (Fig EV4C). However, their interactions with Armi, SoYb, and Vret were maintained (Fig EV4D). These findings strongly suggest the importance of Yb–Yb interaction via the Hel-C domain in the phase separation of Yb bodies, transposon-repressing *flam*-piRNA biogenesis, and transposon silencing.

The $flam^{BG}$ mutants contain artificial *P*-element insertions in front of the *flam* cluster [7,40]. The transcription of the *flam* cluster was completely impaired in $flam^{BG}$ ovaries. Strikingly, Yb bodies were barely detected in $flam^{BG}$ ovaries [13]. RNAi-based depletion of Nxt1 in the ovaries, which should interfere with *flam* RNA export, also caused a severe reduction in *flam*-piRNA accumulation and impaired Yb body formation [13]. These findings suggest that Yb body assembly greatly depends on the expression levels of the *flam* cluster *in vivo*. We propose that Yb bodies are multivalent RNA–protein condensates whose assembly depends on Yb self-association (*i.e.*, protein–protein association) and Yb–*flam* transcript association (*i.e.*, RNA–protein association).

The $flam^{KG}$ mutants contain artificial *P*-element insertions within the *flam* cluster, reducing *flam* transcripts significantly [7,40]. Our analysis of published piRNA sequences showed that *flam*-piRNAs were barely detected in $flam^{KG}$ ovaries, as reported previously (Fig 4E) [10]. In contrast, the levels of *tj*-piRNAs were high (Fig 4E). These results strongly support the concept that Yb body formation is not mandatory for non-transposon-repressing piRNA production.

Conclusion

Here, we determined the hierarchy of protein components in Yb body assembly and the distinct functions of the Hel-C and eTud domains of Yb. We also determined how all three domains of Yb, the Hel-C, RNA helicase, and eTud domains, cooperatively function in Yb body formation, piRNA biogenesis, and transposon silencing (Fig 4F). A previous genetic study claimed that all of the regions of Yb are essential for fertility [32], but the link between the different regions and fertility remained unclear. This study successfully uncovered the molecular bases of this link.

Surprisingly, we found that piRNA biogenesis in OSCs took place even without Yb body assembly. However, the products are mostly genic piRNAs, which are considered to be "junk" because they cannot target transposons. Yb bodies were originally thought to be the site of piRNA biogenesis. However, the current study provides new insight; that is, Yb bodies are the elaborative system specialized for producing piRNAs functional in transposon silencing.

We noticed that recombinant Yb *in vitro* oligomerizes without RNAs (unpublished observations by S. Hirakata and M. C. Siomi). Thus, we favor the idea that "minimum size Yb body units" assembling under the detection levels of regular microscopy play a role in genic piRNA production in normal OSCs and also in $flam^{KG}$ ovaries. In normal OSCs, genic piRNA precursors may also be sequestered into Yb bodies together with *flam* RNAs. Determination of the sequences of RNAs residing in Yb bodies in normal OSCs or in the ovaries should elucidate this.

Stress granules are generated through LLPS [41,42], where longer transcripts are more strongly enriched in the granules [43]. This was attributed to the fact that longer RNAs contain higher numbers of RNA–protein binding sites. In fact, the *flam* RNAs contained a great number of Yb binding sites throughout their entirety, while genic piRNA sources contained far fewer Yb binding sites, which

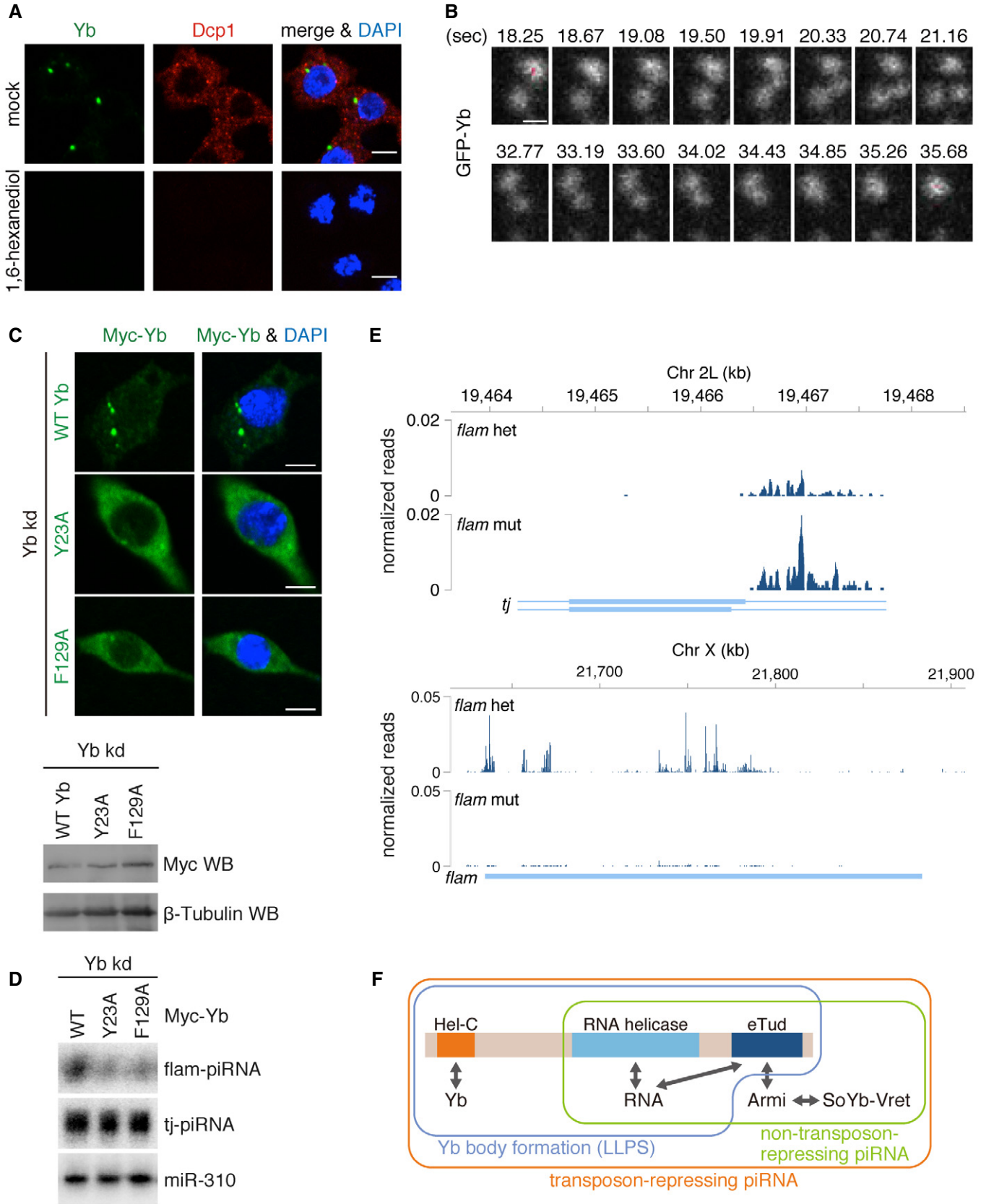

Figure 4.

Figure 4. Yb bodies are phase-separated condensates.

A Yb bodies (Yb in green) disappeared after 1,6-hexanediol treatment of OSCs, as did P bodies (Dcp1 in red). Nuclei are shown in blue. Scale bar: 5 μm.

B Snapshots of live imaging of GFP-Yb expressed in OSCs (Movie EV1). Fusion- and fission-like dynamics of Yb bodies were observed. Saturated pixels are shown in red. Scale bar: 0.5 μm.

C Yb Y23A and F129A mutants (green) impaired Yb body formation. Nuclei are shown in blue. Scale bar: 5 μm.

D Yb Y23A and F129A mutants failed to produce *flam*-piRNAs. miR-310 was used as a loading control.

E Mapping of *flam*- and *tj*-piRNAs produced in the $flam^{KG}$ mutant and heterozygote ovaries.

F Summary of the functionality of each domain of Yb. Production of non-transposon-repressing piRNAs requires RNA helicase and eTud domains of Yb. Yb body formation via LLPS requires all three domains of Yb, but Armi, SoYb, and Vret are dispensable. Production of transposon-repressing piRNAs (*flam*-piRNAs) requires all three domains of Yb and also the Yb body components, Armi, SoYb, and Vret. The Hel-C domain is responsible for Yb–Yb interaction (self-assembly of Yb). The RNA helicase and eTud domains are required for Yb–RNA binding. The eTud domain is also required for Armi binding. Yb binds the SoYb–Vret heterodimer Armi-dependently.

Source data are available online for this figure.

were normally limited in the 3′ UTRs [34]. This difference may be the cause of the enrichment of *flam*, but no other, RNAs in Yb bodies. However, it was difficult to confirm this in this study because the lengths of *flam* RNA isoforms *per se* have not been determined yet. We imagine that sequestering RNAs to Yb bodies in a manner largely dependent on the number of Yb binding sites would be beneficial for cells, as this would avoid the background accumulation of incorrect RNAs to Yb bodies because the incorrect RNAs would be unlikely to have many Yb binding sites.

Our data suggested that the eTud domain of Yb is involved in both Armi binding and RNA binding. Even though the eTud domain generally recognizes symmetrically dimethylated arginine (sDMA) residue of the target protein, Armi lacks motifs for such modification (GRG, ARG, GRA). In addition, the eTud domain of Yb lacks aromatic residues that are responsible for the recognition of sDMA. Therefore, Yb–Armi interaction appears to be mediated by sDMA-independent eTud–protein interaction, as is the case for interaction between BmTDRD12 and Siwi [44]. eTud domain is composed of a Tudor domain and a nuclease-like structure. Because of the nuclease-like folding and the computational prediction that the surface of the eTud domain of Yb is rather basic (unpublished observations by S. Hirakata and M. C. Siomi), we speculate that the eTud domain itself may have the RNA-binding activity.

It is clear that the Hel-C domain is important in Yb body formation. However, the Hel-C domain was predicted to be neither an IDR nor a prion-like domain. Nonetheless, IDRs also confer flexibility on whole protein structures. Therefore, in the case of Yb, having an IDR between the N-terminal Hel-C and the RNA helicase domain may be beneficial for the protein to form multivalent condensates with *flam* RNAs.

Yb bodies are often observed to be surrounded by mitochondria, and piRNA biogenesis most likely occurs at the interface of the two organelles where the piRNA factors and RNA substrates concentrate (Fig EV4E). Providing "liquid-like condensate" properties to Yb bodies would be beneficial for this, allowing increased areas of attachment between the two organelles. The mechanism by which the two organelles are attached is not yet known. Gene screening combined with measuring the distance between Yb bodies and mitochondria may resolve this issue.

Yb bodies are detected not only in the ovaries but also in the testes, where Yb seems to play a role in regulating germline stem cell self-renewal, as it does in the ovaries [32]. However, *yb* null mutant males are fertile; hence, Yb may not be absolutely required in spermatogenesis [45]. This suggests that piRNA biogenesis in males is capable of bypassing Yb. Yb is a member of the TDRD12 family of proteins, in which SoYb is involved. Other species express a counterpart of SoYb but lack one of Yb [44]. The current study clarified that the functions of Yb in *Drosophila* OSCs are as follows: (i) the selection of piRNA precursors, (ii) the induction of piRNA biogenesis, and (iii) the facilitation of production of transposon-repressing piRNAs by assembling Yb bodies. Without these functions, the piRNA pathway would be defective. Thus, identification of Yb counterparts in fly testes and in the gonads of other species is anticipated.

Materials and Methods

Cell lines

Ovarian somatic cells [46] were cultured at 26°C in Shields and Sang M3 medium supplemented with 0.6 mg/ml glutathione, 10% fetal bovine serum (FBS), 10 mU/ml insulin, and 10% fly extract. The fly extract was prepared by heat inactivating the supernatant of homogenized flies (0.2 g/ml adult Oregon R flies in Shields and Sang M3 medium supplemented with 10% FBS) at 60°C for 5 min.

RNAi and transfection with plasmids

RNAi was generally performed as described previously [47]. A total of 5.0×10^6 cells of OSCs and 200 pmol siRNA duplex were suspended in 20 μl of Solution SF of the Cell Line Nucleofector Kit SF (Lonza Bioscience), and electroporation was conducted using program DG-150 of a Nucleofector 96-well Shuttle device (Lonza Bioscience). For transfection with plasmids, 2.5×10^7 OSCs and 1.5–18 μg of plasmids were suspended in 100 μl of buffer (180 mM sodium phosphate buffer for Church and Gilbert hybridization [pH 7.2], 5 mM KCl, 15 mM $MgCl_2$, 50 mM D-mannitol; modified from Ref. [48]) with or without 600 pmol siRNA duplex, and electroporation was conducted in an electroporation cuvette with a 2-mm gap using program N-020 of a Nucleofector 2b device (Lonza Bioscience). In the RNAi experiments, cells were transfected again with siRNA duplex after 48 h and harvested 48 h later. In the rescue assays, endogenous Yb was knocked down by RNAi 48 h before transfection of both plasmids and siRNA, and cells were harvested 72 h later. The sequences of the siRNAs used are shown in Table EV2.

Plasmid construction

Expression vectors of Myc-tagged Yb mutants (ΔHel-C, ΔeTud, Hel-C, Y23A, and F129A) were generated by inverse PCR, using the RNAi-resistant Myc-Yb WT vector [12] as the template. A DNA fragment encoding β-gal was PCR-amplified from pMT/V5-His/*lacZ* (Thermo Fisher Scientific) and cloned into the HindIII-AgeI-digested pAcM vector to generate the expression vector of Myc-tagged β-gal. For the construction of the Myc-BSD vector, a DNA fragment encoding BSD was amplified from the BSD vector [34] and then cloned into linearized pAcM vector generated by PCR using NEBuilder HiFi DNA Assembly Master Mix (New England Biolabs). To yield the expression vectors of Flag-tagged WT Yb and BSD, the regions encoding the Myc tag were deleted from Myc-Yb WT and BSD vectors by inverse PCR, and a DNA fragment encoding a 3 × Flag peptide was inserted using NEBuilder HiFi DNA Assembly Master Mix. The expression vector of Flag-tagged Yb Hel-C was generated from Flag-Yb WT vector by inverse PCR. To generate the GFP-Yb expression vector, a DNA fragment encoding Yb was cloned into the EcoRI-digested pAcE vector [34] using In-Fusion HD Cloning Kit (Takara Bio). The sequences of the primers used are shown in Table EV2.

Immunofluorescence

Immunofluorescence was generally performed as described previously [16]. Cells were fixed with 4% formaldehyde in phosphate-buffered saline (PBS; FUJIFILM Wako Pure Chemical) and permeabilized with 0.1% Triton X-100 in PBS, followed by immunostaining with antibodies diluted in 3% bovine serum albumin (BSA). Cells were washed with PBS after each treatment. The primary antibodies used in this study were anti-Yb monoclonal antibody (1:200 dilution; [12]), anti-Armi monoclonal antibody (1:200 dilution; [16]), anti-Vret monoclonal antibody (1:300 dilution; this study), anti-SoYb monoclonal antibody (1:500 dilution; this study), anti-Myc rabbit polyclonal antibody (1:500 dilution; C3956, Merck), anti-Dcp1 monoclonal antibody (1:200 dilution; [49]), and anti-Piwi monoclonal antibody (1:250; [50]). Monoclonal antibodies for Vret and SoYb were raised in this study using glutathione S-transferase (GST)-tagged Vret (amino acids 1–200) and SoYb (amino acids 1,100–1,300) purified from *E. coli* to immunize mice as described previously [50]. The secondary antibodies used in this study were Alexa 488-conjugated anti-mouse IgG, Alexa 488-conjugated anti-rabbit IgG, Alexa 488-conjugated anti-mouse IgG1, Alexa 488-conjugated anti-mouse IgG2a, Alexa 555-conjugated anti-mouse IgG1, Alexa 555-conjugated anti-mouse IgG2a, and Alexa 555-conjugated anti-mouse IgG2b (all from Thermo Fisher Scientific). All secondary antibodies were used at 1:1,000 dilution. The cells were mounted with VECTASHIELD Mounting Medium with DAPI (Vector Laboratories), followed by observation using an LSM 710 laser scanning confocal microscope (Carl Zeiss). More than 15 cells were analyzed, and representative images are shown.

Subcellular localization of Shu

Expression vectors of GFP-Shu or Shu-GFP [19] were transfected into OSCs using X-fect Transfection Reagent (Takara Bio). Cells were fixed and permeabilized 48 h after transfection in the same manner as the immunofluorescence described above and mounted with VECTASHIELD Mounting Medium with DAPI. The fluorescence of GFP and DAPI was analyzed using an LSM 710 laser scanning confocal microscope.

Western blotting

Western blotting was carried out as described previously [51]. Proteins separated on sodium dodecyl sulfate (SDS) polyacrylamide gels were blotted on nitrocellulose membranes. The membranes were blocked with 5% skimmed milk in 0.1% Tween-20 in PBS (T-PBS) followed by incubation with antibodies diluted in T-PBS. The membranes were extensively washed with T-PBS after each procedure. The primary antibodies used in this study were anti-Yb monoclonal antibody (1:1,000 dilution; [12]), anti-Armi monoclonal antibody (1:1,000 dilution; [16]), anti-Vret monoclonal antibody (1:1,000 dilution; this study), anti-SoYb monoclonal antibody (1:1,000 dilution; this study), anti-Myc rabbit polyclonal antibody (1:1,000 dilution; C3956, Merck), anti-Myc monoclonal antibody (1:1,000 dilution; 9E10, FUJIFILM Wako Pure Chemical), anti-Flag monoclonal antibody (1:10,000 dilution; FLA-1, Medical & Biological Laboratories), and anti-β-tubulin monoclonal antibody (1:1,000 dilution; E7, Developmental Studies Hybridoma Bank). Peroxidase-conjugated anti-mouse IgG (1:5,000 dilution; Cappel) and anti-rabbit IgG (1:1,000 dilution; Cell Signaling Technology) antibodies were used as secondary antibodies. The membranes were incubated with Clarity Western ECL Substrate (Bio-Rad), and images were collected using ChemiDoc XRS Plus System (Bio-Rad).

Immunoprecipitation

Immunoprecipitation was primarily performed as described previously [16]. Cell lysate was prepared in binding buffer [50 mM Tris–HCl (pH 8.0), 150 mM potassium acetate, 5 mM magnesium acetate, 5 mM dithiothreitol (DTT), 0.1% NP-40, 2 μg/ml leupeptin, 2 μg/ml pepstatin A, 0.5% aprotinin, 10% glycerol] and incubated with anti-Armi [16], anti-Vret (this study), or anti-Myc mouse monoclonal antibody bound to Dynabeads Protein G (Thermo Fisher Scientific) at 4°C for 2 h. The beads were washed five times with binding buffer. Eluted proteins were separated on SDS polyacrylamide gels and detected by Western blotting (see above) or silver staining using SilverQuest Silver Staining Kit (Thermo Fisher Scientific).

CLIP

Cross-linking and immunoprecipitation was performed essentially as described previously [34]. Ovarian somatic cells were UV cross-linked by irradiating them uncovered with 200 mJ/cm^2 of 254 nm UV. Immunoprecipitation was performed as described above, following treatment with 10 U/μl RNase T1 (Thermo Fisher Scientific). Beads were washed three times with wash buffer [50 mM Tris–HCl (pH 8.0), 300 mM NaCl, 1 mM DTT, 0.05% NP-40, 2 μg/ml leupeptin, 2 μg/ml pepstatin A, 0.5% aprotinin], and then three times with high-salt wash buffer [50 mM Tris–HCl (pH 8.0), 500 mM NaCl, 1 mM DTT, 0.05% NP-40, 2 μg/ml leupeptin, 2 μg/ml pepstatin A, 0.5% aprotinin]. Dephosphorylation of the 3′ ends of RNAs generated by RNase T1 cleavage was omitted because we did not require

adapter ligation. The 5′ ends of the RNAs were radiolabeled with ^{32}P in binding buffer using T4 polynucleotide kinase (New England Biolabs), followed by NuPAGE (Thermo Fisher Scientific) and ldetection using a Typhoon FLA 9500 (GE Healthcare). For CLIP-qPCR, 0.04 U/μl RNasin Plus RNase Inhibitor (Promega) was added to lysate instead of RNase T1. RNAs were eluted from beads with proteinase K. Total RNAs in aliquots of the lysate were prepared using ISOGEN-LS (NIPPON GENE), following proteinase K treatment. RNAs were treated with DNase before qRT–PCR.

qRT–PCR

Total RNAs were isolated from OSCs using ISOGEN II (NIPPON GENE), followed by DNase treatment. A total of 1 μg of total RNA was reverse-transcribed using a ReverTra Ace qPCR RT Master Mix (TOYOBO), and the resulting cDNAs were amplified with PowerUp SYBR Green Master Mix (Thermo Fisher Scientific) using StepOnePlus (Thermo Fisher Scientific). The sequences of the primers used are shown in Table EV2. Cells were prepared by three independent transfection experiments.

Prediction of domain structure, prion-like domains, and disordered regions

The domain structure of Yb, excluding the eTud domain, was re-predicted using the newer version of HHpred (version 2; [52]) with pfam30 as the HMM database and Psiblast as the MSA generation method, as described previously [17]. The prion-like domains and disordered regions of Yb were predicted by PLAAC [53] and PONDR-FIT [54], respectively.

Small RNA isolation from the immunopurified Piwi complex

To isolate piRNAs in rescue experiments, we transfected 6 μg of expression vectors of Flag-tagged Piwi [23] together with Yb vectors. Cell lysate was prepared in Piwi-binding buffer [20 mM HEPES buffer (pH 7.3), 150 mM NaCl, 2 mM $MgCl_2$, 1 mM DTT, 0.1% NP-40, 2 μg/ml leupeptin, 2 μg/ml pepstatin A, 0.5% aprotinin] with 0.04 U/μl RNasin Plus RNase Inhibitor and incubated with anti-Flag monoclonal antibody bound to Dynabeads Protein G at 4°C for 2 h. The beads were washed five times with Piwi-binding buffer. RNAs were eluted from beads with phenol–chloroform and precipitated with ethanol. For library preparation, RNAs of 23–30 nucleotides in length were eluted from the gels and cloned manually based on the manufacturer's instructions for the TruSeq Small RNA Sample Prep Kit (Illumina), as previously described [47]. For quantification, RNAs were dephosphorylated and ^{32}P-labeled using Antarctic Phosphatase (New England Biolabs) and T4 polynucleotide kinase, respectively, and then separated on a denaturing polyacrylamide gel. Autoradiographs were obtained using Typhoon FLA 9500, and signal intensities were calculated using ImageJ (National Institutes of Health).

piRNA-Seq analysis

Sequencing of piRNA libraries was performed using MiSeq (Illumina) with MiSeq Reagent Kit v3 (Illumina). Adapter-trimmed reads equal to or longer than 18 nucleotides in length were mapped against the *Drosophila* genome (BDGP Release 6 + ISO1 MT/dm6) with FlyBase gene model (Release 6.21) using STAR [55]. Uniquely mapped reads with up to two mismatches were used for further analysis. Reads mapped to transposons and genes were counted using HTSeq [56]. For transposon annotation, the annotation file of repeat sequences was obtained from RepeatMasker (dm6—Apr 2006—RepeatMasker open-4.0.6—Dfam 2.0) and transposons were extracted without distinction between I-int and LTR. Reads mapped to exons of coding genes but not overlapping with repeat sequences, tRNAs, rRNAs, snRNAs, snoRNAs, pseudogenes, ncRNAs, and pre-miRNAs were counted as genic piRNAs using annotation files obtained from RepeatMasker (for repeat sequences) and FlyBase (for the other features). Merged reads of biological duplicates were normalized to one million mapped reads and used for analysis. Genes with low reproducibility in read counts were omitted manually. For visualization of mapped reads, Integrated Genomics Viewer [57] was used.

Mapping of small RNA-Seq reads

Datasets of small RNA-seq obtained from $flam^{KG}$ mutant and heterozygote ovaries (GSE15186; [10]) were used for mapping. Reads of 23–29 nucleotides after adapter trimming were mapped against the *Drosophila* genome (BDGP Release 6 + ISO1 MT/dm6) with FlyBase gene model (Release 6.21) using STAR. Uniquely mapped reads with up to two mismatches were visualized using Integrated Genomics Viewer. Reads were normalized to read counts of endogenous siRNAs described previously [10].

1,6-Hexanediol treatment

Ovarian somatic cells were treated with 2 μg/ml digitonin with or without 10% 1,6-hexanediol (FUJIFILM Wako Pure Chemical) in Shields and Sang M3 medium at 26°C for 1 h. Endogenous Yb and Dcp-1 were detected by immunofluorescence as described above.

Live imaging of GFP-Yb in OSCs

Ovarian somatic cells transfected with the expression vector of GFP-Yb were plated in 35-mm film-bottomed dishes (Matsunami) and incubated for 24 h. Live-cell imaging was conducted on a confocal laser scanning microscope FV3000 (OLYMPUS) using a 100×/1.4-NA (numerical aperture) oil-immersion objective (OLYMPUS) with either single confocal slices or z stacks. The resulting single images were analyzed using Olympus Fluoview (OLYMPUS).

Northern blotting

Northern blotting was carried out as described previously [34]. Total RNAs were isolated from OSCs using ISOGEN II, followed by DNase treatment. RNAs separated on denaturing polyacrylamide gels were blotted on uncharged nylon membranes. The membranes were cross-linked using chemical cross-linking solution (160 mM 1-ethyl-3-(3-dimethylaminopropyl) carbodiimide (EDC), 130 mM 1-methylimidazole (pH 8.0); [58]) at 60°C for 1 h and then incubated at 42°C for 30 min in hybridization buffer [200 mM sodium phosphate buffer (pH 7.2), 7% SDS, 1 mM ethylenediaminetetraacetic acid (EDTA)] as a pre-hybridization treatment. Oligonucleotide probes were ^{32}P-labeled using T4 polynucleotide kinase and hybridized to the membrane in hybridization buffer at 42°C overnight. The

membranes were washed in saline sodium citrate buffer [30 mM sodium citrate (pH 7.0), 300 mM NaCl] supplemented with 0.1% SDS at 42°C, and autoradiographs were obtained using Typhoon FLA 9500. The sequences of the probes used are shown in Table EV2.

Quantification and statistical analysis

Quantification of transposons was carried out by the $\Delta\Delta C_t$ method using datasets obtained by three independent transfection experiments. In the CLIP-qPCR experiment, enrichment was calculated by the percent input method and normalized to *tj* mRNA. Data are presented as the mean ± SEM. For comparisons, an unpaired two-tailed Student's *t*-test was performed using StatPlus (AnalystSoft). $P < 0.05$ were considered as significant. In the piRNA-seq analysis, R with the pspearman package was used to calculate the Spearman's rho and *P*-values to analyze the correlation between the two datasets. *P*-values for all comparisons in the piRNA-seq analysis were calculated to be $< 2.2 \times 10^{-16}$.

Data availability

piRNA-seq data have been deposited at the GEO database (http://www.ncbi.nlm.nih.gov/geo/) under accession number GSE121605.

Expanded View for this article is available online.

Acknowledgements
We thank J. Brennecke for Shu expression vectors and T. Tajima (OLYMPUS Corporation) for assistance with live imaging. We are grateful to T. Hirose and T. Yamazaki for experimental suggestions and discussions. We also thank other members of the Siomi laboratories for discussions and comments on the manuscript. This work was supported by grants from the Ministry of Education, Culture, Sports, Science and Technology of Japan to H.I. and M.C.S. S.H. is supported by the Japan Society for the Promotion of Science.

Author contributions
AF and YT determined the hierarchical manner in Yb body assembly by immunoprecipitation and immunofluorescence, respectively. YT generated monoclonal antibodies. HI performed live imaging of GFP–Yb in OSCs. SH performed the other experiments. SH, HI, and MCS designed the experiments. SH and MCS wrote the manuscript. MCS supervised all the research.

Conflict of interest
The authors declare that they have no conflict of interest.

References

1. Yamashiro H, Siomi MC (2018) PIWI-interacting RNA in *Drosophila*: biogenesis, transposon regulation, and beyond. *Chem Rev* 118: 4404 – 4421
2. Iwasaki YW, Siomi MC, Siomi H (2015) PIWI-interacting RNA: its biogenesis and functions. *Annu Rev Biochem* 84: 405 – 433
3. Juliano C, Wang J, Lin H (2011) Uniting germline and stem cells: the function of Piwi proteins and the piRNA pathway in diverse organisms. *Annu Rev Genet* 45: 447 – 469
4. Malone CD, Hannon GJ (2009) Small RNAs as guardians of the genome. *Cell* 136: 656 – 668
5. Ghildiyal M, Zamore PD (2009) Small silencing RNAs: an expanding universe. *Nat Rev Genet* 10: 94 – 108
6. Aravin AA, Hannon GJ, Brennecke J (2007) The Piwi-piRNA pathway provides an adaptive defense in the transposon arms race. *Science* 318: 761 – 764
7. Brennecke J, Aravin AA, Stark A, Dus M, Kellis M, Sachidanandam R, Hannon GJ (2007) Discrete small RNA-generating loci as master regulators of transposon activity in *Drosophila*. *Cell* 128: 1089 – 1103
8. Lau NC, Robine N, Martin R, Chung WJ, Niki Y, Berezikov E, Lai EC (2009) Abundant primary piRNAs, endo-siRNAs, and microRNAs in a *Drosophila* ovary cell line. *Genome Res* 19: 1776 – 1785
9. Li C, Vagin VV, Lee S, Xu J, Ma S, Xi H, Seitz H, Horwich MD, Syrzycka M, Honda BM *et al* (2009) Collapse of germline piRNAs in the absence of Argonaute3 reveals somatic piRNAs in flies. *Cell* 137: 509 – 521
10. Malone CD, Brennecke J, Dus M, Stark A, McCombie WR, Sachidanandam R, Hannon GJ (2009) Specialized piRNA pathways act in germline and somatic tissues of the *Drosophila* ovary. *Cell* 137: 522 – 535
11. Goriaux C, Desset S, Renaud Y, Vaury C, Brasset E (2014) Transcriptional properties and splicing of the *flamenco* piRNA cluster. *EMBO Rep* 15: 411 – 418
12. Murota Y, Ishizu H, Nakagawa S, Iwasaki YW, Shibata S, Kamatani MK, Saito K, Okano H, Siomi H, Siomi MC (2014) Yb integrates piRNA intermediates and processing factors into perinuclear bodies to enhance piRISC assembly. *Cell Rep* 8: 103 – 113
13. Dennis C, Brasset E, Sarkar A, Vaury C (2016) Export of piRNA precursors by EJC triggers assembly of cytoplasmic Yb-body in *Drosophila*. *Nat Commun* 7: 13739
14. Dennis C, Zanni V, Brasset E, Eymery A, Zhang L, Mteirek R, Jensen S, Rong YKS, Vaury C (2013) "Dot COM", a nuclear transit center for the primary piRNA pathway in *Drosophila*. *PLoS One* 8: e72752
15. Olivieri D, Sykora MM, Sachidanandam R, Mechtler K, Brennecke J (2010) An *in vivo* RNAi assay identifies major genetic and cellular requirements for primary piRNA biogenesis in *Drosophila*. *EMBO J* 29: 3301 – 3317
16. Saito K, Ishizu H, Komai M, Kotani H, Kawamura Y, Nishida KM, Siomi H, Siomi MC (2010) Roles for the Yb body components Armitage and Yb in primary piRNA biogenesis in *Drosophila*. *Genes Dev* 24: 2493 – 2498
17. Handler D, Olivieri D, Novatchkova M, Gruber FS, Meixner K, Mechtler K, Stark A, Sachidanandam R, Brennecke J (2011) A systematic analysis of *Drosophila* TUDOR domain-containing proteins identifies Vreteno and the Tdrd12 family as essential primary piRNA pathway factors. *EMBO J* 30: 3977 – 3993
18. Zamparini AL, Davis MY, Malone CD, Vieira E, Zavadil J, Sachidanandam R, Hannon GJ, Lehmann R (2011) Vreteno, a gonad-specific protein, is essential for germline development and primary piRNA biogenesis in *Drosophila*. *Development* 138: 4039 – 4050
19. Olivieri D, Senti KA, Subramanian S, Sachidanandam R, Brennecke J (2012) The cochaperone Shutdown defines a group of biogenesis factors essential for all piRNA populations in *Drosophila*. *Mol Cell* 47: 954 – 969
20. Preall JB, Czech B, Guzzardo PM, Muerdter F, Hannon GJ (2012) Shutdown is a component of the *Drosophila* piRNA biogenesis machinery. *RNA* 18: 1446 – 1457
21. Handler D, Meixner K, Pizka M, Lauss K, Schmied C, Gruber FS, Brennecke J (2013) The genetic makeup of the *Drosophila* piRNA pathway. *Mol Cell* 50: 762 – 777
22. Vagin VV, Yu Y, Jankowska A, Luo Y, Wasik KA, Malone CD, Harrison E, Rosebrock A, Wakimoto BT, Fagegaltier D *et al* (2013) Minotaur is critical for primary piRNA biogenesis. *RNA* 19: 1064 – 1077

23. Yashiro R, Murota Y, Nishida KM, Yamashiro H, Fujii K, Ogai A, Yamanaka S, Negishi L, Siomi H, Siomi MC (2018) Piwi nuclear localization and its regulatory mechanism in *Drosophila* ovarian somatic cells. *Cell Rep* 23: 3647 – 3657
24. Brower-Toland B, Findley SD, Jiang L, Liu L, Yin H, Dus M, Zhou P, Elgin SC, Lin H (2007) *Drosophila* PIWI associates with chromatin and interacts directly with HP1a. *Genes Dev* 21: 2300 – 2311
25. Sienski G, Dönertas D, Brennecke J (2012) Transcriptional silencing of transposons by Piwi and Maelstrom and its impact on chromatin state and gene expression. *Cell* 151: 964 – 980
26. Dönertas D, Sienski G, Brennecke J (2013) *Drosophila* Gtsf1 is an essential component of the Piwi-mediated transcriptional silencing complex. *Genes Dev* 27: 1693 – 1705
27. Ohtani H, Iwasaki YW, Shibuya A, Siomi H, Siomi MC, Saito K (2013) DmGTSF1 is necessary for Piwi-piRISC-mediated transcriptional transposon silencing in the *Drosophila* ovary. *Genes Dev* 27: 1656 – 1661
28. Sienski G, Batki J, Senti KA, Dönertas D, Tirian L, Meixner K, Brennecke J (2015) Silencio/CG9754 connects the Piwi-piRNA complex to the cellular heterochromatin machinery. *Genes Dev* 29: 2258 – 2271
29. Yu Y, Gu J, Jin Y, Luo Y, Preall JB, Ma J, Czech B, Hannon GJ (2015) Panoramix enforces piRNA-dependent cotranscriptional silencing. *Science* 350: 339 – 342
30. Iwasaki YW, Murano K, Ishizu H, Shibuya A, Iyoda Y, Siomi MC, Siomi H, Saito K (2016) Piwi modulates chromatin accessibility by regulating multiple factors including histone H1 to repress transposons. *Mol Cell* 63: 408 – 419
31. Sato K, Siomi MC (2018) Two distinct transcriptional controls triggered by nuclear Piwi-piRISCs in the *Drosophila* piRNA pathway. *Curr Opin Struct Biol* 53: 69 – 76
32. Szakmary A, Reedy M, Qi H, Lin H (2009) The Yb protein defines a novel organelle and regulates male germline stem cell self-renewal in *Drosophila melanogaster*. *J Cell Biol* 185: 613 – 627
33. Homolka D, Pandey RR, Goriaux C, Brasset E, Vaury C, Sachidanandam R, Fauvarque MO, Pillai RS (2015) PIWI slicing and RNA elements in precursors instruct directional primary piRNA biogenesis. *Cell Rep* 12: 418 – 428
34. Ishizu H, Iwasaki YW, Hirakata S, Ozaki H, Iwasaki W, Siomi H, Siomi MC (2015) Somatic primary piRNA biogenesis driven by *cis*-acting RNA elements and *trans*-acting Yb. *Cell Rep* 12: 429 – 440
35. Pandey RR, Homolka D, Chen KM, Sachidanandam R, Fauvarque MO, Pillai RS (2017) Recruitment of Armitage and Yb to a transcript triggers its phased processing into primary piRNAs in *Drosophila* ovaries. *PLoS Genet* 13: e1006956
36. Qi H, Watanabe T, Ku HY, Liu N, Zhong M, Lin H (2011) The Yb body, a major site for Piwi-associated RNA biogenesis and a gateway for Piwi expression and transport to the nucleus in somatic cells. *J Biol Chem* 286: 3789 – 3797
37. Banani SF, Lee HO, Hyman AA, Rosen MK (2017) Biomolecular condensates: organizers of cellular biochemistry. *Nat Rev Mol Cell Biol* 18: 285 – 298
38. Luo Y, Na Z, Slavoff SA (2018) P-bodies: composition, properties, and functions. *Biochemistry* 57: 2424 – 2431
39. Strome S (2005) *Specification of the germ line*, pp 1 – 10. Pasadena, CA: WormBook
40. Mével-Ninio M, Pelisson A, Kinder J, Campos AR, Bucheton A (2007) The *flamenco* locus controls the *gypsy* and *ZAM* retroviruses and is required for *Drosophila* oogenesis. *Genetics* 175: 1615 – 1624
41. Molliex A, Temirov J, Lee J, Coughlin M, Kanagaraj AP, Kim HJ, Mittag T, Taylor JP (2015) Phase separation by low complexity domains promotes stress granule assembly and drives pathological fibrillization. *Cell* 163: 123 – 133
42. Wheeler JR, Matheny T, Jain S, Abrisch R, Parker R (2016) Distinct stages in stress granule assembly and disassembly. *eLife* 5: e18413
43. Khong A, Matheny T, Jain S, Mitchell SF, Wheeler JR, Parker R (2017) The stress granule transcriptome reveals principles of mRNA accumulation in stress granules. *Mol Cell* 68: 808 – 820
44. Pandey RR, Tokuzawa Y, Yang Z, Hayashi E, Ichisaka T, Kajita S, Asano Y, Kunieda T, Sachidanandam R, Chuma S *et al* (2013) Tudor domain containing 12 (TDRD12) is essential for secondary PIWI interacting RNA biogenesis in mice. *Proc Natl Acad Sci USA* 110: 16492 – 16497
45. King FJ, Lin H (1999) Somatic signaling mediated by *fs(1)Yb* is essential for germline stem cell maintenance during *Drosophila* oogenesis. *Development* 126: 1833 – 1844
46. Saito K, Inagaki S, Mituyama T, Kawamura Y, Ono Y, Sakota E, Kotani H, Asai K, Siomi H, Siomi MC (2009) A regulatory circuit for *piwi* by the large Maf gene *traffic jam* in *Drosophila*. *Nature* 461: 1296 – 1299
47. Sumiyoshi T, Sato K, Yamamoto H, Iwasaki YW, Siomi H, Siomi MC (2016) Loss of *l(3)mbt* leads to acquisition of the ping-pong cycle in *Drosophila* ovarian somatic cells. *Genes Dev* 30: 1617 – 1622
48. Nye J, Buster DW, Rogers GC (2014) The use of cultured *Drosophila* cells for studying the microtubule cytoskeleton. *Methods Mol Biol* 1136: 81 – 101
49. Miyoshi K, Okada TN, Siomi H, Siomi MC (2009) Characterization of the miRNA-RISC loading complex and miRNA-RISC formed in the *Drosophila* miRNA pathway. *RNA* 15: 1282 – 1291
50. Saito K, Nishida KM, Mori T, Kawamura Y, Miyoshi K, Nagami T, Siomi H, Siomi MC (2006) Specific association of Piwi with rasiRNAs derived from retrotransposon and heterochromatic regions in the *Drosophila* genome. *Genes Dev* 20: 2214 – 2222
51. Miyoshi K, Tsukumo H, Nagami T, Siomi H, Siomi MC (2005) Slicer function of *Drosophila* Argonautes and its involvement in RISC formation. *Genes Dev* 19: 2837 – 2848
52. Söding J, Biegert A, Lupas AN (2005) The HHpred interactive server for protein homology detection and structure prediction. *Nucleic Acids Res* 33: W244 – W248
53. Lancaster AK, Nutter-Upham A, Lindquist S, King OD (2014) PLAAC: a web and command-line application to identify proteins with prion-like amino acid composition. *Bioinformatics* 30: 2501 – 2502
54. Xue B, Dunbrack RL, Williams RW, Dunker AK, Uversky VN (2010) PONDR-FIT: a meta-predictor of intrinsically disordered amino acids. *Biochim Biophys Acta* 1804: 996 – 1010
55. Dobin A, Davis CA, Schlesinger F, Drenkow J, Zaleski C, Jha S, Batut P, Chaisson M, Gingeras TR (2013) STAR: ultrafast universal RNA-seq aligner. *Bioinformatics* 29: 15 – 21
56. Anders S, Pyl PT, Huber W (2015) HTSeq–a Python framework to work with high-throughput sequencing data. *Bioinformatics* 31: 166 – 169
57. Thorvaldsdóttir H, Robinson JT, Mesirov JP (2013) Integrative Genomics Viewer (IGV): high-performance genomics data visualization and exploration. *Brief Bioinform* 14: 178 – 192
58. Pall GS, Hamilton AJ (2008) Improved northern blot method for enhanced detection of small RNA. *Nat Protoc* 3: 1077 – 1084
59. Chirn GW, Rahman R, Sytnikova YA, Matts JA, Zeng M, Gerlach D, Yu M, Berger B, Naramura M, Kile BT *et al* (2015) Conserved piRNA expression from a distinct set of piRNA cluster loci in eutherian mammals. *PLoS Genet* 11: e1005652
60. Klein JD, Qu C, Yang X, Fan Y, Tang C, Peng JC (2016) c-Fos repression by Piwi regulates *Drosophila* ovarian germline formation and tissue morphogenesis. *PLoS Genet* 12: e1006281
61. Hahn MW, Han MV, Han SG (2007) Gene family evolution across 12 *Drosophila* genomes. *PLoS Genet* 3: e197